Stochastic boundary conditions to the convection-diffusion equation including chemical reactions at solid surfaces

P. Szymczak* and A. J. C. Ladd†

Department of Chemical Engineering, University of Florida, Gainesville, Florida 32611-6005, USA
(Received 22 July 2003; published 30 March 2004)

Simulations of heat and mass transport may require complex nonlinear boundary conditions to describe the flow of mass and energy across an interface. Although stochastic methods do not suffer from the numerical diffusion of grid-based methods, they typically lose accuracy in the vicinity of interfacial boundaries. In this work we introduce ideas and algorithms to account for mass (or energy) transfer at reactive interfaces, with accuracies comparable to the bulk phase. We show how to introduce particles into the system with the correct distribution near the interface, as well as the correct flux through the interface. The algorithms have been tested in a channel flow, for which accurate numerical solutions can be independently calculated.

I. INTRODUCTION

Surface chemical reactions, involving deposition and dissolution of molecular species, are controlled by the transport of reactants and products as well as by the intrinsic chemical kinetics. The two dominant transport mechanisms, convection and diffusion, frequently produce quite different dynamics and structures within the system. We will consider systems containing a reactive solid surface $\mathcal{S}$, which might, for example, be the surface of a biological cell, the porous matrix of a specimen of limestone, or a corroding metal surface. The transport of chemical species in the surrounding fluid is described by the convection-diffusion equation

$$\partial_t c_i + \mathbf{u} \cdot \nabla c_i = D_i \nabla^2 c_i, \tag{1}$$

where c_i is the concentration of species i, D_i is its diffusion coefficient, and $\mathbf{u}$ is the fluid velocity field. The essential assumption here is that the chemical concentrations are sufficiently small that they do not affect either the diffusion coefficient or the fluid velocity, which is then determined solely by the solid geometry and external boundary conditions on the flow.

Stochastic methods have long been used to solve problems in heat transport [1–3] and neutron transport [4], because of the ease with which these methods can be adapted to complex interfaces. An extensive bibliography of applications is contained in Ref. [3]. Stochastic methods have also been applied to bulk-phase reaction-diffusion systems [5,6], and to the dispersion of passive tracers in a porous medium [7–9]. Recently, a stochastic method was used to calculate the flux of reactive tracers between complex fractured surfaces [10]. Although stochastic methods can lead to accurate solutions of the convection-diffusion equation in bulk phases, they typically lose accuracy in the region of interfacial boundaries. For example, the algorithms used in Ref. [7–10] introduce errors proportional to the square-root of the

time step in the vicinity of an interface [11,12]. However, in recent work [12] we developed second-order implementations of the zero-flux and constant concentration boundary conditions. Although we were not able to solve the boundary-condition problem for a completely general flow field, we were able to obtain quadratic convergence in two of the most important cases; a local shear flow parallel to the surface and a uniform flow across the interface. In this paper we propose generalizations of these ideas to situations where there are chemical reactions at the interface, which can include spatially varying nonlinear rate laws. Although we only explicitly consider mass transfer in this paper, the same algorithms can also be applied to stochastic simulations of heat transfer.

The paper is organized as follows. In Sec. II we briefly summarize our previous work. In Sec. III we introduce the different types of boundary condition that are encountered in systems with surface mass transport, and a method to measure the concentration in the vicinity of the interface is described in Sec. III B. Stochastic implementations of these boundary conditions in the presence of a linear shear flow are constructed in Sec. IV. The implementations are tested in Sec. V, and conclusions are given in Sec. VI.

II. REFLECTION AND ABSORPTION

A stochastic process $\mathbf{X}(t)$, associated with the convection-diffusion equation [Eq. (1)] obeys the stochastic differential equation

$$d\mathbf{X} + \mathbf{v}(\mathbf{X})dt = \sqrt{2D}d\mathbf{W}, \tag{2}$$

where $d\mathbf{W}$ is the differential of a Wiener process with unit variance. We use a Heun predictor-corrector method to solve Eq. (2);

$$\mathbf{X}^p(t+\Delta t) = \mathbf{X}(t) + \mathbf{v}[\mathbf{X}(t)]\Delta t + \sqrt{2D}\Delta \mathbf{W}(t),$$

$$\mathbf{X}(t+\Delta t) = \mathbf{X}(t) + \frac{1}{2}\{\mathbf{v}[\mathbf{X}(t)] + \mathbf{v}[\mathbf{X}^p(t+\Delta t)]\}\Delta t$$

$$+ \sqrt{2D}\Delta \mathbf{W}(t), \tag{3}$$

*On leave from Institute of Theoretical Physics, Warsaw University, 00-681 Hoża 69, Poland.
†Email address: ladd@che.ufl.edu

where the increment $\Delta \mathbf{W}(t) = \mathbf{W}(t + \Delta t) - \mathbf{W}(t)$ is a Gaussian random variable with variance Δt, and is the same for both predictor and corrector steps. The Heun method can be shown to be weakly second-order convergent [13,14], meaning that, if $\mathbf{X}_{ex}$ is an exact trajectory, then the error in any polynomial function of $\mathbf{X}$ is bounded by

$$|\langle g[\mathbf{X}_{ex}(t)] - g[\mathbf{X}(t)] \rangle| \leq \delta(\Delta t)^2, \qquad (4)$$

where δ is a positive constant.

In a previous paper [12] we developed and tested stochastic algorithms to solve the convection-diffusion equation in the vicinity of reflecting and absorbing boundaries:

$$\hat{\mathbf{n}}(\mathbf{r}) \cdot \nabla c(\mathbf{r}) = 0, \quad \mathbf{r} \in \mathcal{S}, \qquad (5)$$

$$c(\mathbf{r}, t) = 0, \quad \mathbf{r} \in \mathcal{S}, \qquad (6)$$

where $\hat{\mathbf{n}}(\mathbf{r})$ is a unit vector normal to the surface. Although we were not able to solve the problem for a general flow field, we constructed second-order approximations to the stochastic processes near reflecting and absorbing walls for two physically relevant flow fields: a linear shear flow, which is characteristic of the flow near a solid interface, and a locally uniform flow, which occurs near an inflow or outflow boundary. In the latter case we also generalized Eq. (6) to include a constant nonzero concentration.

Near a solid boundary, an incompressible flow can be approximated by a linear shear flow

$$v_y = \gamma x, \qquad (7)$$

with a velocity gradient γ normal to the surface $x = 0$. In order to determine the convective contribution to the tangential (y) displacement, we must integrate over all possible trajectories between the initial and final x positions. The average tangential displacement can then be computed by introducing a weighting function $p(\tilde{x}|x, x', \Delta t)$ [12]

$$p(\tilde{x}|x, x', \Delta t) = \frac{\displaystyle\int_0^{\Delta t} G(x, \tilde{x}, \Delta t - t) G(\tilde{x}, x', t) dt}{G(x, x', \Delta t) \Delta t}, \qquad (8)$$

where $G(x, x', t)$ is the one-dimensional diffusion propagator. The quantity $p(\tilde{x}|x, x', \Delta t) \Delta t$ is the mean time the particle spends at a position $\tilde{x}$ during its move from x' to x in the time step Δt. The weight function turns out to be uniform in the region between x' to x, but with tails that account for indirect paths from x' to x. A typical distribution of $p(\tilde{x}|x, x', \Delta t)$ is shown in Fig. 5 of Ref. [12]; the unit of length in this paper is chosen to be the root-mean-square displacement in unit time, $\sqrt{2D}$, as before.

In the vicinity of the wall, a reflection must be applied to the negative ($\tilde{x} < 0$) part of the function so that in this case the proper weight function p_r is (see Fig. 1)

$$p_r(\tilde{x}|x, x', \Delta t) = p(\tilde{x}|x, x', \Delta t) + p(-\tilde{x}|x, x', \Delta t), \qquad (9)$$

and is limited to the region ($\tilde{x} > 0$). The average convective velocity $\bar{v}_y$, during the time step Δt, can be calculated by
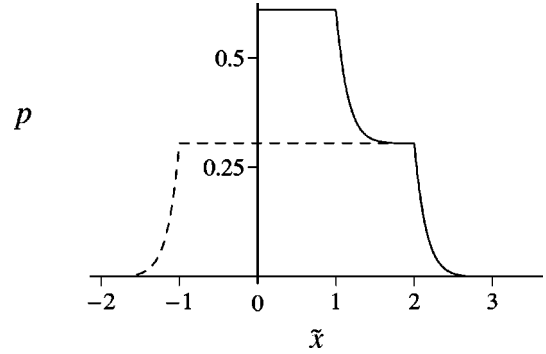

FIG. 1. The conditional probability distribution $p_r(\tilde{x}|x, x', \Delta t)$ for a trajectory beginning at $x' = 2$ and ending at $x = -1$ behind the wall (which is reflected to the point $x = 1$) [Eq. (8)].

integrating the flow field $v_y = \gamma x$ at each $\tilde{x}$, using $p_r(\tilde{x}|x, x', \Delta t)$ as the weight function,

$$\bar{v}_y = \gamma \int_0^\infty \tilde{x} p_r(\tilde{x}|x, x', \Delta t) d\tilde{x}, \qquad (10)$$

although the final expression is quite lengthy. If the source and receiver positions are not too close to the wall the average velocity reduces to the mean of the source and receiver velocities, as in Eq. (3). The details of the implementation can be found in Ref. [12].

A zero-concentration (absorbing) boundary condition can be implemented by modifying this scheme so that reflected particles are converted into holes, carrying negative mass in the overall concentration balance. A virtual distribution of particles can be constructed to simulate a constant-concentration reservoir at an inflow or outflow boundary. Again the details of the implementation, together with examples, can be found in Ref. [12].

To save computational time, boundary conditions are only applied to particles close to the interface, the critical distance, d_c, being of the order of the rms displacement. We fully expect that these boundary conditions can be applied to curved surfaces by dividing them into locally flat regions, for example by triangulation. If the distance from the source point to the nearest face is less than d_c, the particle is advected according to Eq. (10) with the distances x and x' measured with respect to that face. Since this algorithm ignores the curvature of the interface, it is necessary to ensure that d_c is smaller than the characteristic length scale of the surface features. In the vicinity of a corner a reflected trajectory may encounter more than one surface in a single time step. In this case we have found [12] that the algorithm appropriate to each interface can be applied sequentially, at each successive encounter with a bounding surface. For example, a specular reflection at a reflecting wall followed by reflection plus conversion to holes at an absorbing one. This is simple to implement in the absence of the flow or when the convection is included to the first order in Δt. Second-order corrections for the flow are difficult to implement near a sharp corner, where the flow field is no longer a simple shear. However, in this case the first nonvanishing contribution to the flow field is quadratic in the distance from the surface and a first-order method is sufficient.

III. MASS-TRANSFER BOUNDARY CONDITIONS

In this paper we will investigate more complex boundary conditions describing mass transfer due to chemical reactions at the interface:

$$\mathbf{J}_i = f_i(c_1, c_2, \dots)\hat{\mathbf{n}}, \tag{11}$$

where $\mathbf{J}_i$ is the flux of species i across the boundary, $c_1, c_2, \dots$ are the concentrations of the respective species at the boundary, and $\hat{\mathbf{n}}(\mathbf{r})$ denotes a unit normal pointing into the fluid. Conservation of mass leads to the boundary condition

$$-D_i \nabla c_i(\mathbf{r}) \cdot \hat{\mathbf{n}}(\mathbf{r}) = f(c_1(\mathbf{r}), c_2(\mathbf{r}), \dots), \quad \mathbf{r} \in \mathcal{S}. \tag{12}$$

The convective contribution to the flux vanishes at a solid surface and is omitted from Eq. (12).

There are two qualitatively different cases contained in Eq. (12), depending on the sign of f_i.

(1) $f_i(c_1, c_2, \dots) > 0$. Particles are added to the fluid (dissolution).

(2) $f_i(c_1, c_2, \dots) < 0$. Particles are removed from the fluid (deposition).

Although surface reaction rates may depend on several concentrations, from now on we consider only a single component in describing our implementation of the various boundary conditions; the generalization to multicomponent systems is straightforward. In this section we will consider purely diffusive transport, for which the Green's functions near a planar interface are known analytically. In Sec. IV we will generalize these results to a linear shear flow.

A. Dissolution

A mass transfer boundary condition specifies the flux of particles, $f(c_0)\hat{\mathbf{n}}$, entering or leaving the system; f is prescribed by the chemical kinetics at the surface and c_0 is the concentration at the surface $c(\mathbf{r} \in \mathcal{S})$. The mass flux can be generated by distributing an appropriate number of particles along the interface, but the numerical implementation must lead to the correct concentration profile near the interface as well. We first consider one-dimensional diffusion with a dissolving interface at $x = 0$, and show that the correct boundary condition corresponds to a continuous (in time) concentration source of strength

$$s(x) = f(c_0)\delta(x). \tag{13}$$

In the absence of the flow, such a source produces the concentration profile

$$c^s(x, t + \Delta t)$$

$$= f(c_0) \int_{t'=0}^{\Delta t} 2G(x, 0, t')dt'$$

$$= \frac{f(c_0)}{D}\left[\sqrt{\frac{4D\Delta t}{\pi}}e^{-x^2/4D\Delta t} - x\,\mathrm{Erfc}\left(\frac{x}{\sqrt{4D\Delta t}}\right)\right] \tag{14}$$

where it has been assumed that the concentration at the wall, c_0, is essentially unchanged during the time step Δt. At the same time the particles already in the system are reflected at the $x = 0$ wall. The total concentration profile is then

$$c(x, t + \Delta t)$$

$$= c^s(x, t + \Delta t)$$

$$+ \int_0^\infty [G(x, x', \Delta t) + G(x, -x', \Delta t)]c(x', t)dx', \tag{15}$$

which is the solution of the diffusion equation with an initial concentration profile $c(x, t)$ and boundary conditions $\partial_x c(0) = -f(c_0)/D$ and $c(\infty) = 0$. The derivative of the concentration profile in Eq. (15),

$$\frac{\partial c}{\partial x} = -\frac{f(c_0)}{D}\mathrm{Erfc}\left(\frac{x}{\sqrt{4D\Delta t}}\right), \tag{16}$$

matches the required flux $f(c_0)$ at $x = 0$. It then follows that a linear profile $c_0 - xf(c_0)/D$ is stationary near the dissolving wall.

In multidimensional systems, a continuous particle source again generates a matching particle flux and concentration gradient. For example, in a two-dimensional system bounded by a dissolving wall $x = 0$, with a spatially varying flux across the interface $f[c_0(y)]$,

$$\lim_{x \to 0} \partial_x c(x, y, t + \Delta t)$$

$$= \lim_{x \to 0} \partial_x c^s(x, y, t + \Delta t)$$

$$= \lim_{x \to 0} \partial_x \int_{t'=0}^{\Delta t} dt \int_{-\infty}^{\infty} dy' \frac{1}{4\pi Dt}e^{-\frac{x^2 + (y-y')^2}{4Dt}}f[c_0(y')]$$

$$= -\int_{-\infty}^{\infty} dy' \frac{f[c_0(y')]}{2\pi D}\lim_{x \to 0}\partial_x \mathrm{Ei}\left(-\frac{x^2 + (y-y')^2}{4D\Delta t}\right)$$

$$= -\int_{-\infty}^{\infty} dy' \frac{f[c_0(y')]}{D}e^{-\frac{(y-y')^2}{4D\Delta t}}\lim_{x \to 0}\frac{1}{\pi}\frac{x}{x^2 + (y-y')^2}$$

$$= -\frac{f[c_0(y)]}{D}. \tag{17}$$

In implementing a continuous dissolution process, it is not sufficient to simply ensure that the correct number of particles, $f(c_0)\Delta t dS$, are introduced through the surface element dS. For example, introducing the particles at the beginning of each time step, rather than continuously throughout the time step, produces a concentration profile with vanishing normal derivative at the wall, as shown in Fig. 2. Moreover discrete dissolution of particles even fails to maintain the correct stationary state, as shown in Fig 3.

The above analysis suggests the following procedure for implementing mass transfer boundary conditions, which incorporates continuous dissolution.

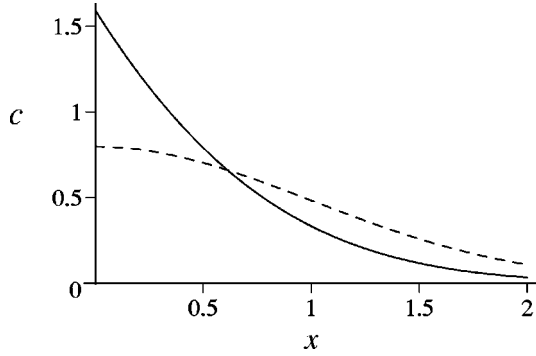(1) Divide the interface into a number of cells ΔS_i.

FIG. 2. Discrete (dashed) vs continuous (solid) dissolution. In the discrete case, a particle concentration $c(x) = \delta(x)$ is placed on a reflecting wall at $t=0$. In the continuous case, particles are released uniformly over the time step $\Delta t = 1$. The graphs show the concentration profiles $c(x,1)$.

(2) Determine the concentrations of the individual species at the center of each cell, $\mathbf{r}_i$, (see Sec. III B), and calculate the fluxes $\mathbf{J}(\mathbf{r}_i) = f[c(\mathbf{r}_i)]\hat{\mathbf{n}}(\mathbf{r}_i)$ according to Eq. (11).

(3) Distribute particles in the surface element ΔS_i around $\mathbf{r}_i$. The exact distribution of particles depends on the order of the approximation scheme. It is usually sufficient to include only linear variations in concentration along the surface, so that

$$f[c(\mathbf{r})] = f[c(\mathbf{r}_i)] + (\mathbf{r} - \mathbf{r}_i) \cdot \nabla_{\parallel} f[c(\mathbf{r}_i)], \quad \mathbf{r}, \mathbf{r}_i \in \Delta S_i, \tag{18}$$

where $\nabla_{\parallel}$ indicates a derivative along the interface.

(4) Advance the source particles with a time step picked from a uniform random distribution in the range $[0, \Delta t]$, to simulate continuous dissolution. Advance the particles in the bulk by Δt, using specular reflection at the solid surfaces.

B. Measuring the concentration profile at the interface

In order to determine the interfacial fluxes in Eq. (11), the concentration profile of each species is required along the
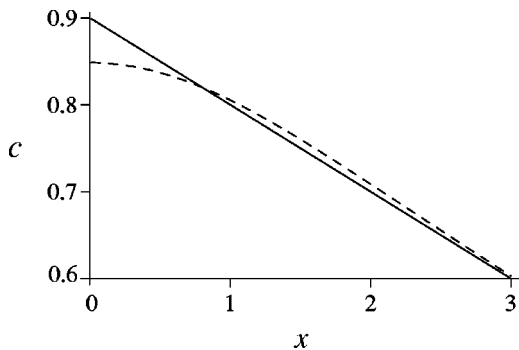

FIG. 3. Concentration profiles near a solid wall. A linear concentration profile (solid line), $c(x,0) = c_0 - [f(c_0)/D]x$, with $f(c_0) = -r(c_0 - c_s)$ and parameters $c_s = 1$, $c_0 = 0.9$, and $r = 0.1$ is advected for a single step ($\Delta t = 1$). The concentration profile $c(x,1)$ is shown for continuous dissolution (solid line) and discrete dissolution (dashed line). In the latter case the linear profile is unsteady.

system boundaries. We have investigated several possible methods of measuring the concentration, and the method presented below is the most accurate scheme we have discovered so far. It is also robust and relatively simple to implement. First we discretize the system boundaries: for example, on the $x=0$ interface, mesh points are of the form $(0, y_k)$ with $0 = y_0 < y_1 < \cdots < y_{n-1} < y_n = L_y$. This divides the wall into n cells, $C_1, C_2, \ldots, C_n$, with C_i extending from y_{i-1} to y_i. The location of each element is taken to be the center of cell C_i,

$$y_i^c = \frac{1}{2}(y_i + y_{i-1}). \tag{19}$$

In order to determine the concentration profile on $x=0$, we measure the concentration profile in the vicinity of the boundary by taking moments:

$$W_{n_1, n_2}^i = \frac{1}{hw_i} \sum_i x^{n_1}(y - y_i^c)^{n_2}, \tag{20}$$

where $w_i = y_i - y_{i-1}$ is the width of the ith cell and the sum is over all particles in the region $0 < x < h$, $y_{i-1} < y < y_i$. The value of h is empirically chosen as a compromise between statistical errors, which are minimized by large values of h, and systematic errors, which are minimized by small values of h.

Given a set of moments W_{n_1, n_2}^i, with $n_1, n_2 \leq m$, the concentration and concentration gradients can be determined. The concentration around a cell i, located on the boundary $x=0$, is expanded in a Taylor series

$$c^i(x,y) = c_0^i + c_x^i x + c_y^i(y - y_i^c) + \cdots, \tag{21}$$

where the concentration $c_0^i = c(0, y_i^c)$ and derivatives $c_x^i = c_x(0, y_i^c)$ and $c_y^i = c_y(0, y_i^c)$ are determined at the center of the cell, $(0, y_i^c)$. In the zeroth approximation the concentration in cell i is assumed to be uniform in the y direction and given by $W_{0,0}^i$ with errors of order h. Solving the moment equations to first order gives

$$c_0^i = 4W_{0,0}^i - 6h^{-1}W_{1,0}^i, \tag{22}$$

$$c_y^i = 12w^{-2}W_{0,1}^i, \tag{23}$$

with errors of order h^2. More involved expressions can be derived at second order and beyond, and in general the error is of order h^{m+1}. Higher order schemes give more precise results provided that enough particles are used to calculate the moments (20). However, increasing the number of tracer particles is computationally expensive and so only first- and second-order schemes are used in this work.

To make a comparison of different order measurements, we have inserted 5×10^6 particles, distributed in the region $0 < x < h$ near the $x=0$ wall with probability $P(x,y) \propto \sqrt{y} e^{-(x+y)}$. Figure 4 shows measurements of the concentration profile on a uniform mesh $y_n = n/10$, $n = 0, 1, \ldots, 10$. It can be seen that wherever the profile changes sufficiently slowly both first- and second-order
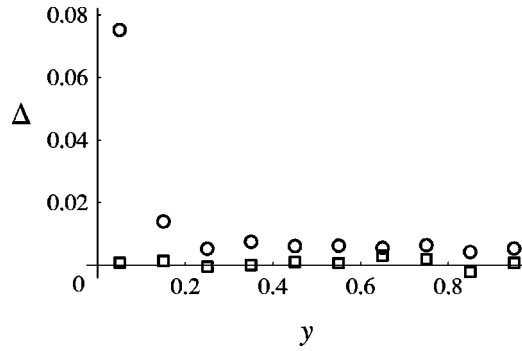
FIG. 4. Concentration profile from first-order (circles) and second-order (squares) moment methods. The solid symbols indicate the normalized difference between the measured concentration at the center of the ith cell, c^i, and the analytic solution c^i_{ex}: $\Delta = (c^i - c^i_{ex})/c^i_{ex}$. There is a substantial increase in the error near $y = 0$ where the derivative is singular.

methods give accurate results. However, as $y \rightarrow 0$, where the distribution has a singular derivative, it is difficult to obtain an accurate profile from the first-order technique.

C. Deposition

In a chemically reacting system, particles can also be deposited at an adsorbing wall, often in combination with the dissolution of other species. The deposition boundary condition, $f(c_0) < 0$ in Eq. (12), can be implemented in an exactly analogous fashion to the dissolving interface by introducing "holes," or particles of negative mass. The addition of holes has the same effect on the concentration field in the bulk region $\mathcal{V}$ as removal of particles from the same locations, but it is simpler to construct the correct distribution near an interface by the addition of holes than by the removal of particles. It can be shown that this algorithm has the same properties as the dissolution algorithm described in Sec. III A. It produces the correct mass flux across the interface and a linear distribution with the appropriate slope is again stationary.

The trajectories of particles and holes are constructed from the same increment distributions and the concentration field is then determined by the difference between the particle and hole concentrations. Particles and holes can be cancelled in the bulk phase to reduce statistical fluctuations [12]. In Sec. IV we will show how the dissolution and deposition boundary conditions can be modified, along the lines developed in Ref. [12], to take account of a linearly varying flow field. In the remainder of this section we will discuss alternative approaches, which have more limited applicability, but which may be useful in some circumstances.

D. Linear kinetic laws

The simplest model for the dissolution of a solid species has a linear kinetic law $f(c_0) = r(c_s - c_0)$, where c_s is the saturation concentration and r is a positive rate constant. Material dissolves or deposits depending on whether the concentration in the solution next to the interface is less than or greater than the saturation concentration. Heat transfer at an interface can also be described by a similar rate law. If the surface kinetics are linear, then it is possible to construct an algorithm that does not require a measurement of the surface concentration, c_0.

The Green's function for the one dimensional diffusion equation with boundary condition

$$-D\left(\frac{\partial c}{\partial x}\right)_{x=0} = -rc_0 \qquad (24)$$

has the form

$$G_d(x,x',\Delta t) = \frac{1}{\sqrt{4\pi D \Delta t}}(e^{-(x-x')^2/4D\Delta t} + e^{-(x+x')^2/4D\Delta t})$$

$$- \frac{r}{D}e^{r(r\Delta t + x + x')/D}\mathrm{Erfc}\left(\frac{x+x'+2r\Delta t}{\sqrt{4D\Delta t}}\right), \qquad (25)$$

where Erfc is the complementary error function. The boundary condition in Eq. (24) implies that the total mass of tracer particles decreases, so that

$$M_0(x',t) = \int_0^\infty G_d(x,x',t)dx < 1. \qquad (26)$$

The mass of each reflected particle must therefore be rescaled by the factor $M_0(x',\Delta t)$, to account for deposition of material at the boundary. The new location of a particle already at x' is sampled from the probability distribution $G_d(x,x',\Delta t)/M_0(x',t)$. A constant flux of particles, rc_s is added to the interface to account for the dissolution flux. The key advantage is that no concentration measurements are required, and this algorithm is therefore as accurate as the other reflection algorithms (for zero flux and zero concentration). However, it can only be implemented with a linear functional form for $f(c_0)$ and cannot account for more general surface kinetics.

E. Finite-range increments

It is not essential that $\Delta \mathbf{W}$ be a Gaussian increment in order to obtain weak convergence. For example, any random variable with the correct second moment guarantees weak first-order convergence of the approximation scheme [13]. Finite-range increments are frequently used [1,7,9] because they are simpler and faster than Gaussian-sampled increments. However, near an interface *any* non-Gaussian increment reduces the order of local convergence to 1/2 [11,12], and does not guarantee global convergence even in the $\Delta t \rightarrow 0$ limit. As a result, the dissolution algorithm with non-Gaussian increments does not lead to the correct steady state, as can be seen in Fig. 5. This contrasts with the case of reflecting and absorbing boundaries, where non-Gaussian increments immediately impose the correct boundary condition [12].

Nevertheless, it is possible to construct an algorithm that leads to the correct stationary distribution, even with non-
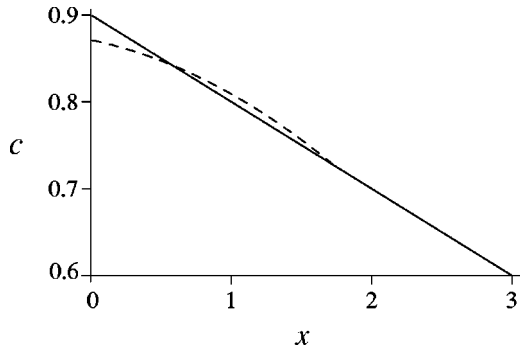
FIG. 5. Concentration profiles near a solid wall. A linear concentration profile (solid line), $c(x,0)=c_0-[f(c_0)/D]x$, with $f(c_0)=r(c_s-c_0)$ and parameters $c_s=1$, $c_0=0.9$, and $r=0.1$ is advected for a single step ($\Delta t=1$). The concentration profile $c(x,1)$ is shown for continuous dissolution with Gaussian increments (solid line) and with increments distributed uniformly in $[-\sqrt{3},\sqrt{3}]$ (dashed line). In the latter case the linear profile turns out to be unsteady.

Gaussian increments. Let us again consider one-dimensional diffusion with a reacting interface at $x=0$. Instead of a continuous source placed on the interface, we construct a virtual distribution of instantaneous sources $c_v(x)$ in a region behind the wall, $x<0$. The gradient in c_v is chosen to generate the desired particle flux across the interface. When these "virtual" particles are propagated using an infinite space Green's function $G(x-x',\Delta t)$, their concentration profile at $t+\Delta t$ is

$$c_v(x,t+\Delta t)=\int_{-\infty}^{0}dx'\,G(x-x',\Delta t)c_v(x',t). \quad (27)$$

After propagation, particles moving into the region $\mathcal{V}$ ($x>0$) are retained whereas those outside $\mathcal{V}$ ($x<0$) are removed from further consideration. Note that virtual particles need only be placed in a small region $[-x_{max},0]$ behind the wall, where x_{max} is the maximum increment.

The distribution $c_v(x)$ is constructed so that, on average, $f(c_0)\Delta t$ virtual particles cross the wall into the region $\mathcal{V}$ in one time step,
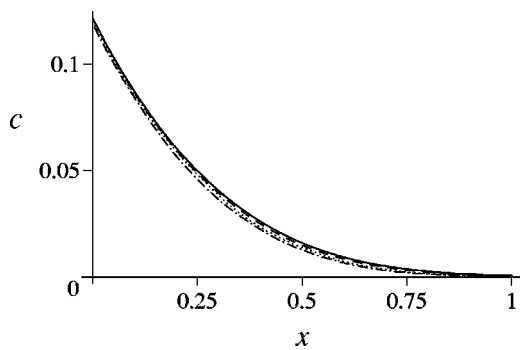
$$c_v(x,t)=-2\frac{f(c_0)}{D}x, \quad x<0. \quad (28)$$

A linear concentration profile $c_0-f(c_0)x/D$ is then stationary; after one time step,

$$
\begin{aligned}
c(x,t+\Delta t)&=\int_0^{\infty}[G(x,x',\Delta t)+G(x,-x',\Delta t)]\\
&\quad\times\left[c_0-\frac{f(c_0)}{D}x'\right]dx'\\
&\quad-\int_{-\infty}^{0}G(x,x',\Delta t)2\frac{f(c_0)}{D}x'dx'\\
&=c_0-\int_{-\infty}^{\infty}G(x,x',\Delta t)\frac{f(c_0)}{D}x'=c_0-\frac{f(c_0)}{D}x,
\end{aligned}
$$

$$(29)$$

where it has *only* been assumed that the propagator is translationally invariant and satisfies the first moment condition $\int_{-\infty}^{\infty}G(x,x',\Delta t)(x-x')dx'=0$.

For Gaussian increments, the distribution of virtual particles $c_v(x,t+\Delta t)$ [Eq. (27)] is exactly the same as the incremental concentration profile for continuous dissolution (Sec. III A). The key advantage of the virtual particle method is that the correct stationary state can be obtained by any translationally invariant propagator. The method can be generalized to more than one spatial dimension by including gradients along the interface into the virtual particle distribution (28) [cf. Eq. (18)]. However, we have not been able to generalize this method to include a fluid flow field, at least at this point in time. Therefore, in the remainder of the paper we will consider continuous dissolution only, with particles placed on the interface itself and Gaussian increments used to move them.
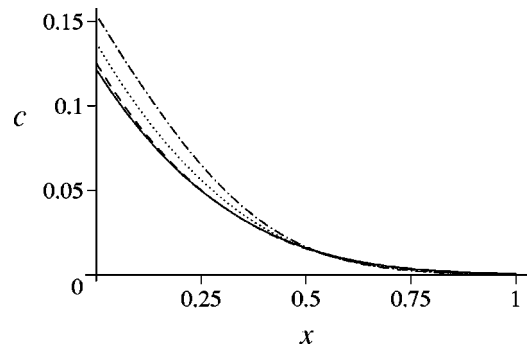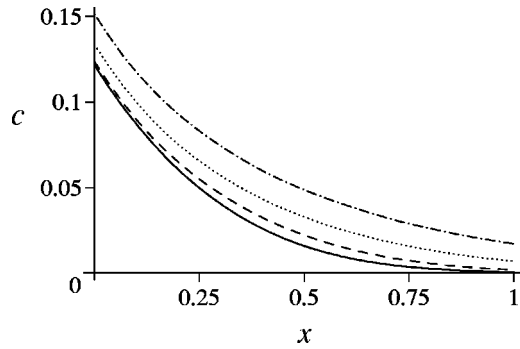

FIG. 6. Continuous dissolution from a point source in a linear shear flow [Eq. (7)] with a Peclet number Pe=10. The source is located at $x=y=0$ on a reflecting wall, $x=0$. The concentration profiles $c(x,0,t=1)$ for $\Delta t=1$ (dash dotted), $\Delta t=0.5$ (dotted) and $\Delta t=0.1$ (dashed) are compared with the exact solution (solid).

FIG. 7. Continuous dissolution from a point source in a linear shear flow [Eq. (7)] with a Peclet number Pe=10. The source is located at $x=y=0$ on a reflecting wall, $x=0$. The concentration profiles $c(x,0,t=1)$ obtained with use of a simplified predictor-corrector scheme for $\Delta t=1$ (dash dotted), $\Delta t=0.5$ (dotted), and $\Delta t=0.1$ (dashed) are compared with the exact solution (solid).

FIG. 8. Continuous dissolution from a point source in a linear shear flow [Eq. (7)] with a Peclet number Pe=10. The source is located at $x=y=0$ on a reflecting wall, $x=0$. The concentration profiles $c(x, 0, t=1)$ obtained with use of a 1st order Euler method for $\Delta t=1$ (dash dotted), $\Delta t=0.5$ (dotted), and $\Delta t=0.1$ (dashed) are compared with the exact solution (solid).

IV. MASS TRANSFER IN THE PRESENCE OF FLOW

The implementation of mass-transfer boundary conditions presented in Sec. III can be generalized to the case of a local shear flow by using the predictor-corrector scheme developed in Ref. [12], which is summarized in Sec. II. The dissolution and deposition fluxes are set up by placing an additional distribution of particles on the interface, as described in Sec. III. The convective contribution to the tangential displacement of the source particles is determined by their normal displacements from the wall at the end of the time step, and by the local shear rate [Eq. (10)].

Figure 6 shows a concentration profile $c(x, 0, t=1)$ produced by a point source located on the wall ($x=0$) in presence of a shear flow [Eq. (7)]. The method is quadratically convergent in Δt, and reasonable results can be obtained even for $\Delta t=0.5$ while for the time step $\Delta t=0.1$ the con-
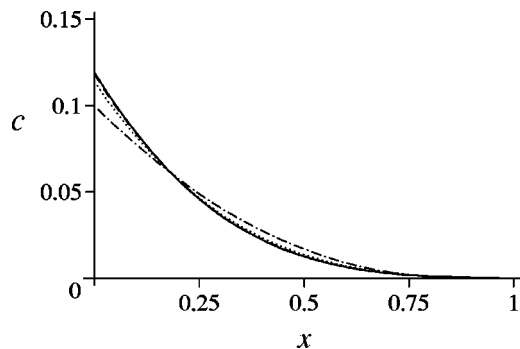

FIG. 9. Continuous dissolution from a point source in a linear shear flow [Eq. (7)] with a Peclet number Pe=10. The source is located at $x=y=0$ on a reflecting wall, $x=0$. The concentration profiles $c(x, 0, t=1)$ were calculated using Gaussian propagators truncated at $2\sqrt{\Delta t}$ (dot dashed), $2.5\sqrt{\Delta t}$ (dotted) and $3\sqrt{\Delta t}$ (dashed). The predictor-corrector method with specular reflection is used to integrate the stochastic differential equations with $\Delta t=1$. The concentration profiles $c(x, 0, 1)$ are compared with the exact solution (solid). The results for truncation distances larger than $3\sqrt{\Delta t}$ are indistinguishable on the scale of the figure from those obtained with a Gaussian distribution.
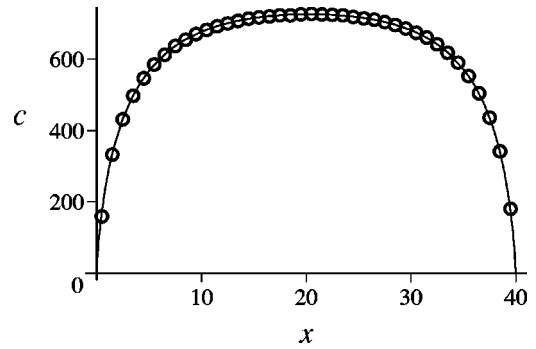

FIG. 10. The concentration profile on a dissolving wall at Peclet number Pe=0.1, as a function of the position along the channel. Random walk simulations (open circles) with a time step $\Delta t=1$ are compared with finite-difference results (solid line).

centration profile is indistinguishable from the exact one on the scale of the figure.

Simpler algorithms are much less accurate and converge only linearly with the time step. Figures 7 and 8 show concentration profiles for the same system, using a simplified predictor corrector method and a first-order Euler scheme respectively. The predictor-corrector method uses the mean velocity at the beginning and end of the time step to estimate the convective displacement. The methods are both linearly convergent in Δt, but the errors in the Euler scheme are much larger and extend deeper into the bulk.

To avoid complications associated with the infinite range of Gaussian propagators, it may prove advantageous to sample diffusive increments of the particles from truncated Gaussian distributions instead. The truncated Gaussian distribution is multiplied by a polynomial in x^2 so as to recover the first two non-zero moments [12]. Figure 9 shows the concentration profile for different truncation distances; for truncations larger than $3\sqrt{\Delta t}$, the dynamics of the random walk are not noticeably affected.

V. CONVECTION-DIFFUSION IN A RECTANGULAR CHANNEL

In this paper we have constructed a consistent set of algorithms that impose a wide range of mass transfer boundary
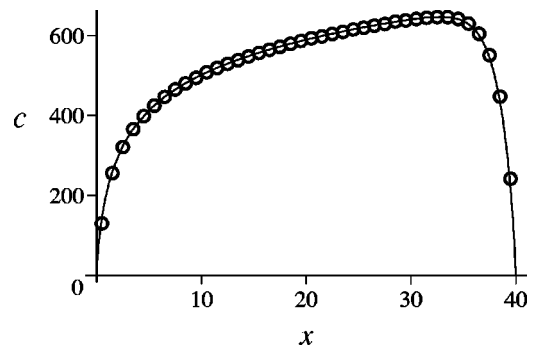

FIG. 11. The concentration profile on a dissolving wall at Peclet number Pe=10, as a function of the position along the channel. Random walk simulations (open circles) with a time step $\Delta t=1$ are compared with finite-difference results (solid line).
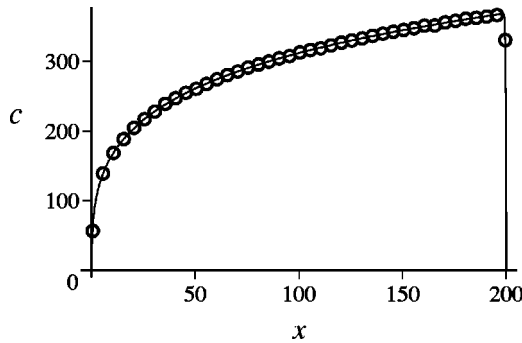
FIG. 12. The concentration profile on a dissolving wall at Peclet number Pe$=1000$, as a function of the position along the channel. Random walk simulations (open circles) with a time step $\Delta t = 0.1$ are compared with finite-difference results (solid line).

FIG. 14. The concentration profile on a dissolving wall at Peclet number Pe$=10$ and Damköhler number Da$=0.2$, as a function of the position along the channel. Random walk simulations (open circles) with a time step $\Delta t = 1$ are compared with finite-difference results (solid line).

conditions. Here the algorithms are tested on two-dimensional convection-diffusion problems whose solution can be found independently. We take a channel of width $L_y = 10$ and length L_x, with a zero concentration inlet and outlet, $c(0,y,t) = c(L_x,y,t) = 0$. The solid wall at $y=0$ is dissolving with kinetics described by the function $f(c_0) = r(c_s - c_0)$, while the wall at $y=L_y$ is absorbing with kinetics described by $f(c_0) = -rc_0$. Here r is the reaction rate while c_s is the saturation concentration ($c_0 < c_s$). We note that dissolution and deposition kinetics possess the important property of negative feedback. An increase in concentration near a dissolving wall leads to a decrease in the dissolution rate, and vice versa, while on an adsorbing wall, an increase in concentration increases the deposition rate. Negative feedback at reactive boundaries is an important stabilizing feature, which improves the accuracy of the numerical solutions because the errors in concentration measurement do not grow with time.

The tests were run from the diffusion-dominated limit Pe $=0.1$, to the convection dominated limit Pe$=1000$. The channel length was increased at higher Peclet numbers, so that the time step can remain large without particles entering and leaving within a single step. The Peclet number Pe $=VL_y/D$ is defined in terms of the velocity at the center of the channel. The rate constant r was taken to be $r=0.1$, which gives a Damköhler number Da$=rL_y/D=2$. For the

Peclet number Pe$=10$, the simulations were run at additional Damköhler numbers Da$=0.2$ (Fig. 14) and Da$=20$ (Fig. 15). We have compared the concentration flux at the absorbing wall with a multi-grid finite-difference code from the NAG library [15].

The results in Figs. 10–15 show that the stochastic simulations are in essentially exact agreement with the finite-difference results over most of the channel, regardless of the Peclet or Damköhler numbers. However, there is a singularity in the concentration field in the corner ($x=0$, $y=0$), where the boundary conditions $c=1$ (along $x=0$) and $c=0$ (along $y=0$) meet. The errors are largest at the highest Peclet number, as shown in Fig. 13. Here the time step must be reduced by a factor of 3 to obtain accurate results in the vicinity of the corner. The time step must also be reduced at high Damköhler number (Da>10, Fig 15), but this is for stability rather than accuracy. If the system is far from equilibrium then there are rapid changes in surface concentration at the beginning of the calculation, while our dissolution-deposition algorithms assume that the change in concentration over a single time step is small. At Da$=20$ we had to reduce the time step by an order of magnitude to obtain a stable solution, but it should be possible to use adaptive
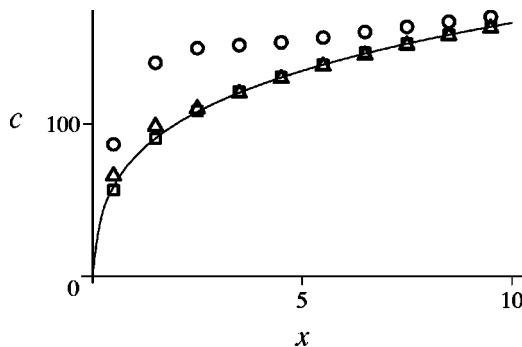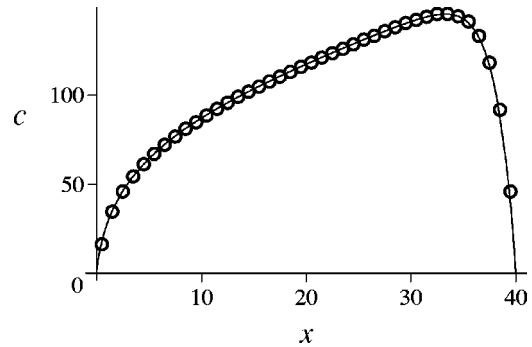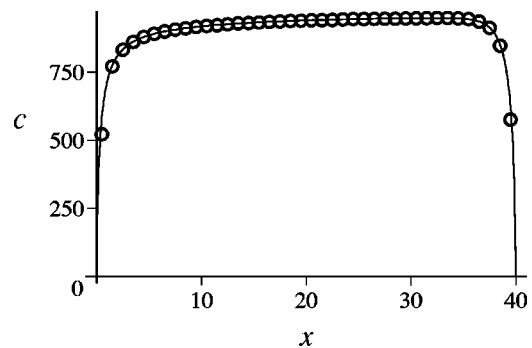

FIG. 13. The concentration profile on a dissolving wall at Peclet number Pe$=1000$ at the inlet of the channel for time steps $\Delta t = 1$ (circles), $\Delta t = 1/3$ (triangles), and $\Delta t = 1/10$ (squares).

FIG. 15. The concentration profile on a dissolving wall at Peclet number Pe$=10$ and Damköhler number Da$=20$, as a function of the position along the channel. Random walk simulations (open circles) with a time step $\Delta t = 0.1$ are compared with finite-difference results (solid line).

methods to increase the time step as the concentration at the interface builds up toward its steady-state value. We note that Da>10 is close to a constant concentration boundary condition, except near the inlet and outlet.

VI. CONCLUSIONS

In this paper we have developed and tested stochastic algorithms to simulate boundary conditions involving mass transfer. Our aim was to develop algorithms that are robust, simple to implement, and flexible with regard to possible chemical kinetics. The key ideas are the introduction of particles with negative mass (holes) to account for deposition kinetics and the sampling of the time step to model continuous dissolution. Combinations of these ideas enable the inclusion of surface chemistry with comparable accuracy to the bulk. Convective transfer near the interface can be included up to second order in Δt, using a sampling of particle paths to calculate the mean convective velocity. We have shown that these algorithms are much more accurate than those generally in use today.

We have tested a multidimensional implementation of the method, using a reactive flow in a rectangular channel, for which precise numerical solutions can be independently calculated. The stochastic simulations are in general indistinguishable from the finite-difference results, except in the vicinity of corners where the concentration gradient is very high. Even under the most extreme conditions, good agreement could be obtained by reducing the time step by a factor of 3–10.

[1] A. Haji-Sheikh and E.M. Sparrow, J. Heat Transfer **122**, 121 (1967).

[2] S.K. Fraley, T.J. Hoffman, and P.N. Stevens, J. Heat Transfer **102**, 121 (1980).

[3] A.F. Ghoniem and F.S. Sherman, J. Comput. Phys. **61**, 1 (1985).

[4] Yu. A. Shreider, *The Monte Carlo Method* (Pergamon Press, Oxford, 1966).

[5] A. J. Chorin, in *Computing Methods in Applied Science and Engineering*, edited by R. Glowinski and J. L. Lions (North-Holland, Amsterdam, 1980), pp. 229–235.

[6] A.S. Sherman and C.S. Peskin, SIAM (Soc. Ind. Appl. Math.) J. Sci. Stat. Comput. **9**, 170 (1988).

[7] J. Salles, J.F. Thovert, R. Delannay, L. Prevors, J.L. Auriault, and P.M. Adler, Phys. Fluids A **5**, 2348 (1993).

[8] T. Rage, Ph.D. thesis, University of Oslo, 1996.

[9] R.S. Maier, D.M. Kroll, R.S. Bernard, S.E. Howington, J.F. Peters, and H.T. Davis, Phys. Fluids **12**, 2065 (2000).

[10] R. Verberg and A.J.C. Ladd, Phys. Rev. E **65**, 016701 (2002).

[11] J. Honerkamp, *Stochastic Dynamical Systems* (VCH, New York, 1993).

[12] P. Szymczak and A. J. C. Ladd, Phys. Rev. E **68**, 036704 (2003).

[13] H. C. Öttinger, *Stochastic Processes in Polymeric Fluids* (Springer-Verlag, Berlin, 1996).

[14] P. E. Kloeden and E. Platen, in *Numerical Solution of Stochastic Differential Equations*, Applications of Mathematics Vol. 23 (Springer, New York, 1992), p. 23.

[15] The Numerical Algorithms Group Limited, Oxford. *NAG Fortran Library Manual, Mark 18*, 1997.